Int. J. Electrochem. Sci., 11 **(2016)** 9175 – 9191, doi: 10.20964/2016.11.73

International Journal of
ELECTROCHEMICAL
SCIENCE
www.electrochemsci.org

Corrosion Inhibition Effect of Histidine and Its Derivatives Self-Assembled Films Formed of 304 Stainless Steel

Zhe Zhang[1,*], *Xiaodong Huang*[1], *Ningchen Tian*[1], *Fusong Ni*[1], *Le Ruan*[1],*Yuzeng Lv*[2], *Ling Wu*[3]

[1] Guangxi Key Laboratory of Electrochemical and Magneto-chemical Functional Materials, College of Chemistry and Bioengineering, Guilin University of Technology, Guilin 541004, PR China
[2] Engineering Research Center of Exploration for hidden Nonferrous and Precious Metal Ore Deposits, Ministry of Education，541004，PR China
[3] School of Chemistry and Chemical Engineering, Shandong University, Jinan 250100, PR China
[*]E-mail: zhangzhe@glut.edu.cn

Received: 10 March 2016 / *Accepted:* 19 September 2016 / *Published:* 10 October 2016

The histidine and its derivatives self-assembled (SA) films were prepared on the 304 stainless steel (SS) surface. EIS and potentiodynamic polarization curves measurements proved that these SA films could effectively protect SS against corrosion in 3.5% NaCl solution, with a maximal protection efficiency of 94.24% achieved by Carbobenzyloxy-L-histidine film. XPS studies confirmed that Carbobenzyloxy-L-histidine molecule could adsorb on SS surface. The quantum chemical calculation and dynamic simulation provided the theoretical support about the inhibition mechanism.

Keywords: histidine; self-assembled films; 304 stainless steel; electrochemical techniques; XPS.

1. INTRODUCTION

With the development of economy, the application of metals is increasing. It's more and more significant that prevent metals from corrosion. In recent years, people have paid more attention to self-assembled (SA) films [1]. SA films have been applied to many aspects of our lives as a new method in corrosion prevention, especially metals as copper [2-6] and iron [7-10]. Many materials can be used in SA films as inorganic materials and organic materials. In recent years, more and more people choose organic materials for high efficiency, environmentally friendliness and the ease of fabrication, measurement, manipulation and characterization [1, 11]. The molecules which form the SA films have polar head groups designed to interact and bind specifically and chemically to the solid surface, especially spontaneous adsorption on metals [12]. Due to the organic molecules always contain the heteroatoms which exhibit high activity as S, O, N, and P for adsorption behavior [13-16]. Aramaki et al. [17-19], prepared two-dimensional polymer films and ultrathin polymer coatings on iron by multistep modification method. Firstly, they assembled SA films in *p*-hydroxymethylbenzene by a covalent bond on iron surface. Secondly, multistep modified the SA films by using tetraethoxysilane and 1,8-octanediol molecules. Lastly making the outermost layer of 1,2-bis (triethoxysilyl) ethane and akyltriethoxysilane molecules. The protective abilities enhanced with the films thickness increasing. Laibinis and Whitesides [20] reported the SA films could inhibit the copper from corrosion based on spontaneous adsorption of n-alkanethiols onto the copper surfaces.

Recently, some amino acid molecules were used as “green” inhibitors to protect metal materials avoid corrosion in various environments [21-23]. Our research group have study the corrosion inhibition efficiency of methionine and its derivatives SA films on 1045 carbon steel in a 3.5% NaCl solution, the *N*-(9-fluorenylmethoxycarbonyl)- L-methionine SA films showed a maximal protection efficiency of 95.01% [24]. L- histidine containing both (-NH_2) and heterocyclic ring groups (shown in Fig. 1a), can be resolved in the natural and save more costing than traditional SAMs. The nitrogen atom in amino acid molecule has a pair of free electron which can prove the adsorption ability of amino acid to form self-assembled films on metal surface [25-27]. Zhang et al. [28], have reported that the protection efficiency of histidine SA films was further improved with the iodide ions adding into the histidine self-assembly solution (pH=10). Mobin et al. [29], have reported that histidine could inhibit the corrosion of mild steel in 0.1 M H_2SO_4 solution, the maximum inhibition efficiency was 71.09% at 30 ^{o}C. And the inhibition efficiency could be synergistically increased in the presence of surfactants, sodium dodecyl sulfate and cetyltrimethyl ammonium bromide.

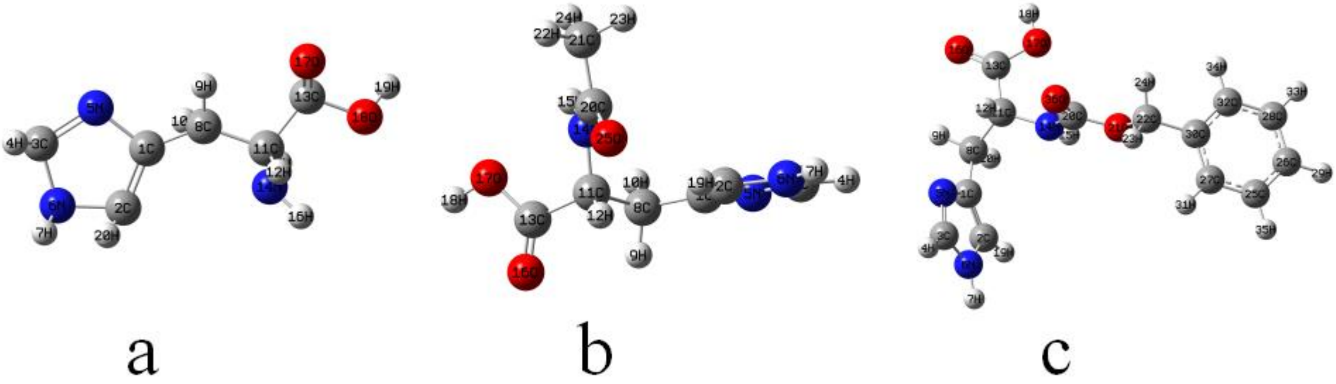

Figure 1. Self-assembled molecules of histidine and its derivatives which from the quantum chemical calcul-ation. L-histidine(a), N-Acetyl-L-histidine (b) and Carbobenzyloxy-L-histidine(c).

The purpose of this work is to investigate the protection effects of 304 stainless steel (SS) in 3.5% NaCl solution by L-histidine (His), N-Acetyl-L-histidine (Ace-His) and Carbobenzyloxy-L-histidine (Cbz-His) SA films, as shown in Fig 1. Electrochemical techniques were used to investigate protection abilities of His and its derivatives on SS electrodes. XPS technique was used to prove the forming of His and its derivatives SA films. The relationship between the molecular structure and inhibition efficiency can be discussed from molecular dynamics (MD) simulation and quantum chemical calculation.

2. EXPERIMENTAL

2.1. Electrodes and self-assembled

The working electrode was prepared using 304 SS, which was a cylindrical rod 3.0 cm long with a cross-sectional area of 0.049 cm^2. The chemical composition of SS (wt%) was C (0.07%), Mn (1.0%), Cr (17.19%), P (0.035%), S (0.03%), Ni (8.11%), Mo (0.03%), Cu (0.03%), Ti (0.03%) and Fe (the remaining 73.47%). The epoxy resin was wrapped up in SS rod and both were embedded in a glass tube, which made that only cross-section exposed in the corrosion solution. Before each test the working electrode was polished with 800#, 1000#, and 1400# grades emery papers and finally degreased with ethanol.

The self-assembled molecules were His, Ace-His and CBZ-His (AR, Aladdin Industrial Corporation). All of the self-assembled molecules were dissolved in doubly distilled water to produce the 0.01 M assembly solution. The basic electrolyte was a 3.5 NaCl solution (wt%) prepared from analytical grade reagent and doubly distilled water.

The cleaned electrodes were immersed in the assembly solution for various time (2 h, 4 h, 6 h, 8 h, 10 h and 12 h) at room temperature of 25℃.

2.2. Electrochemical measurements

Electrochemical measurements based on the traditional electrochemical cell of three electrodes system which contains a working electrode, a saturated calomel electrode (SCE) as the reference electrode and a platinum foil (1.0 cm^2) as counter electrode. A Luggin–Haber capillary belong to the system, too. The electrochemical measurements were performed via an AUTOLAB electrochemical workstation (PGSTA12, Metrohm). Parameters setting of impedance measurements were 5 mV in amplitude of the corrosion potential with a sinusoidal potential perturbation and from 100 kHz to 0.01 Hz of the frequency. The polarization curves were measured by dynamically scanning the potential at 2 $mV \cdot s^{-1}$ from E_{ocp} - 200 mV to E_{ocp} + 200 mV. The temperature condition was controlled via using water bath for 25 ± 2°C and the volume of NaCl solution was 80 mL.

2.3. X-ray photoelectron spectroscopy (XPS)

The steel specimens used for surface morphology examination were SS rod (5.0 mm diameter). The polishing and cleaning methods were the same as above. After immersed in assembly solution for 12 h, the SS was washed by distilled water and anhydrous ethanol. Then, dry the SS at room temperature.

The XPS spectra were performed using ESCALAB 250Xi system (Thermo Electron Corporation, USA). The excitation source was set under Al Kα radiation and at the same time, the photoelectron energy was under 1253.6 eV. Survey scans and relevant core levels were recorded: Fe 2p, C 1s, N 1s, O 1s and S 2p.

2.4. Theory and computational details

Gaussian 03 software can give a result for Quantum chemical calculations [30]. The Density Functional Theory (DFT) method and the B3LYP were all involved in the study. B3LYP is very valuable for geometrical optimizations, which is a performance about the Becke-type three-parameter hybrid together with the gradient-corrected correlation function of Lee, Yang, and Parr [31-33]. The results of Quantum chemical calculations were: the energy of the highest occupied molecular orbital (E_{HOMO}), the energy of the lowest unoccupied molecular orbital (E_{LOMO}), the value of the energy gap ($\triangle E = E_{\mathrm{LOMO}}-E_{\mathrm{HOMO}}$) and the dipole moment (μ).

The Discover module of Materials Studio 6.0 software can give a performance for Molecular dynamic simulations, which came from Accelrys Inc [34]. Controlling by the Andersen thermostat and NVT ensemble, which was set under 298k, setting the time step of 1.0fs, and also at the same time setting the simulation time of 500 ps, employing the COMPASS force field, and then the system was well prepared. The Ewald summation method with a cutoff radius of 9.50 Å,van der Waals and electrostatic interactions was set, which was non-bonding and also as atom-based summations. In the case of investigation the oxide films on SS is consisted of duplex layers，the inner layer of *p*-type semiconductor is a rich-Cr_2O_3 layer and the outer layer of *n*-type is a rich-Fe_2O_3 layer [35-43]. So, the whole simulated system was constructed with a Fe_2O_3 layer and a vacuum inhibitor molecule layer. Fe_2O_3 (1 1 0) surface was selected for studying because the (1 1 0) surface is a densely packed surface and therefore the most stable [44]. The Fe_2O_3 crystal contained 5 layers, and all the atoms of Fe_2O_3 were frozen. In order to make the potential energy to be the lowest total energy in the entire system the geometry of the system have to be optimized. The purpose of molecular dynamic simulations was to make the entire system in a stable equilibrium that the temperature and the energy of the system wave at a stable value. The adsorption intensity of the inhibitor molecules on the Fe_2O_3 (1 1 0) surface of the SS can be expressed by means of the binding energy. The interaction energy $E_{\mathrm{adsorption}}$ between the Fe_2O_3 surface and the inhibitor molecules was calculated according to the following equation (Eq.):

$$E_{\mathrm{adsorption}} = E_{\mathrm{total}} - (E_{\mathrm{surface}} + E_{\mathrm{inhibitors}}) \qquad (1)$$

$$E_{\mathrm{binding}} = -E_{\mathrm{adsorption}} \qquad (2)$$

where E_{surface} is the surface energy of Fe_2O_3 (1 1 0) and $E_{\mathrm{inhibitor}}$ is the energy of the inhibitor molecule. E_{total} is the energy of the entire system contain the Fe_2O_3 crystal and inhibitor molecule adsorbed on it. The energy of binding and the energy of adsorption is opposite in value, shown as in Eq. (2).

3. RESULT AND DISCUSSION

3.1 Electrochemical impedance spectroscopy (EIS)

Fig. 2 shows the impedance spectra of various His and its derivatives SA films modified SS electrode with different assembling time ranged from 0 h to 12 h. All the measured impedance data are analyzed with ZView2 software and the fitted data are listed in Table 1.

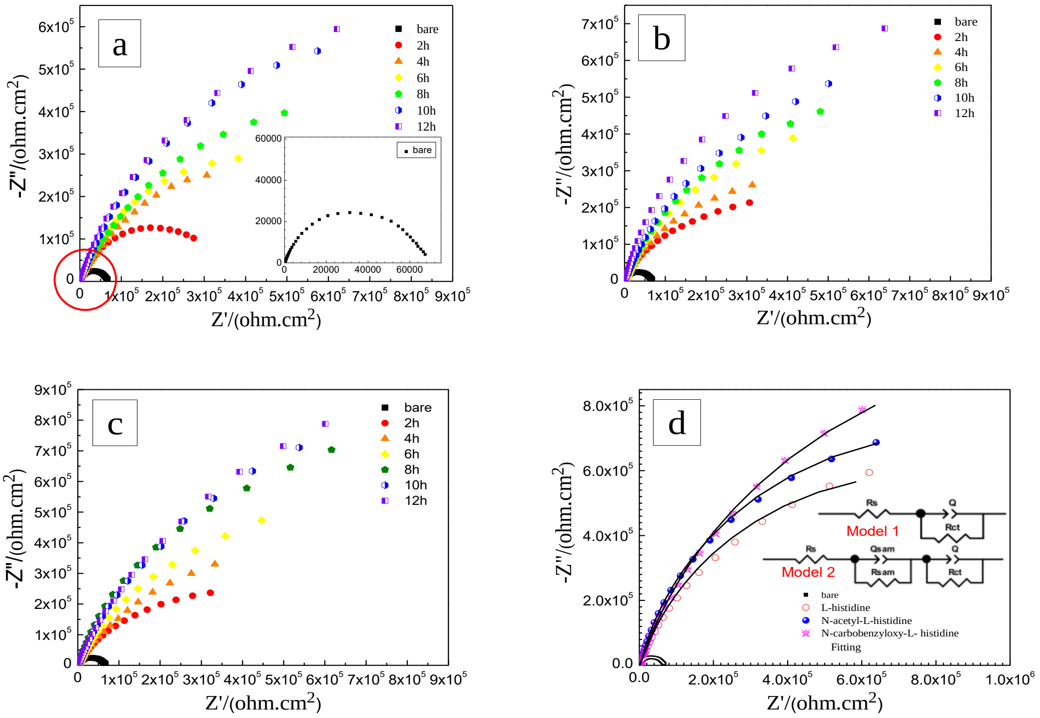

Figure 2. Nyquist impedance spectra of the working electrode with and without SA films formed in 0.01 M His (a), 0.01 M Ace-His (b) and 0.01 M CBZ-His (c) solutions in 3.5% NaCl solutions. The solid lines are their fitted curves.

Fig. 2 presents that the impedance spectrum of bare SS electrode has a similar shape of capacitive loop, due to the dispersion effect and the condition of the electrode surface, the curves are not exact semicircles and to some extents are not as good as assumed [45]. So, the non-homogeneities in the system can be defined using the constant-phase element (Q) [46]. The bare SS working electrode and modified SS working electrode can be described by the using of the models of equivalent circuit in Fig. 2d. The circuit is consist of the electrolyte resistance (R_s), charge transfer resistance (R_{ct}) and constant-phase element (Q) which is associated with the charge transfer process that occurs on the surface of the working electrode, R_{sam} and Q_{sam} are identified with the resistance and capacitance of the SA films. The model 1 is used to fit the measurements date of bare SS working electrode, the model 2 is used to fit the measurements date of modified SS working electrodes.

To determine the impedance parameters of bare SS specimen and the SS specimen modified by His and its derivatives, the inhibition efficiency (η) was calculated by the following equation:

$$\eta_R(\%) = \frac{R_{ct} - R_{ct}^0}{R_{ct}} \times 100\% \qquad (3)$$

where R_{ct}^0 and R_{ct} stand for the charge transfer resistance of bare SS electrode and SA films modified electrodes, respectively. The values of Q capacitance (Q_{dl}) were calculated using Eq. (4) [47-49]:

$$Q_{dl} = Y_0^{1/n} R_{ct}^{(1-n)/n} \qquad (4)$$

where Y_0 and n are the magnitude of the Q and the deviation parameter, respectively.

Table 1. Element values of a circuit equivalent to that in Figure 2 that fit the impedance spectra in Figure 2d and the values of the protection efficiency (η).

Assembly molecules	**Immersion time**	R_S	Q_{sam}		R_{sam}	Q		Q_{dl}	R_{ct}	η_R
			$Y_0\times10^{-4}$	**n**		$Y_1\times10^{-6}$	n_1		$\times10^5$	
	（h）	($\Omega\cdot cm^2$)	($\Omega^{-1}cm^{-2}s^n$)		($\Omega\cdot cm^2$)	($\Omega^{-1}cm^{-2}s^n$)		$\mu F\ cm^{-2}$	($\Omega\cdot cm^2$)	**（%）**
Bare	0	20.42	—	—	—	5.014	0.86		1.476	—
His	2	23.61	0.239	0.673	249.9	9.31	0.779	39.68	3.468	57.43
	4	26.31	0.122	0.756	286.8	12.21	0.817	32.48	6.461	77.15
	6	22.69	0.174	0.77	287	14.28	0.82	24.95	7.366	79.96
	8	30.56	0.3308	0.682	300.1	8.342	0.775	30.13	10	85.24
	10	26.62	0.1616	0.703	320.9	10.46	0.881	20.30	12.97	88.62
	12	26.35	0.534	0.691	331.5	8.798	0.828	24.34	15.25	90.32
Ace-His	2	29.74	0.1032	0.623	201.8	13.3	0.792	50.02	5.441	72.87
	4	25.74	0.2277	0.695	257	16.21	0.806	40.95	6.658	77.83
	6	26.89	0.1924	0.641	300.1	14.31	0.857	32.25	9.102	83.78
	8	23.16	0.1507	0.686	323.7	9.235	0.78	36.19	13.73	89.25
	10	22.42	0.1579	0.676	309.4	9.046	0.787	35.03	16.44	91.02
	12	26.84	0.6215	0.642	331.8	8.812	0.871	21.3	17.3	91.87
Cbz-His	2	28.81	0.1653	0.754	1567	14.15	0.786	63.41	6.192	76.16
	4	28.84	0.2542	0.633	1211	15.21	0.778	47.82	9.791	84.92
	6	24.37	0.3012	0.653	1320	9.301	0.809	31.99	20.13	92.67
	8	25.53	0.1376	0.677	1564	8.526	0.79	34.03	21.41	93.1
	10	27.79	0.138	0.657	1440	10.14	0.831	30.73	22.98	93.57
	12	24.62	0.2055	0.675	1040	6.769	0.818	18.55	25.64	94.24

The capacitive loop diameters of the SS electrode covered with His and its derivatives films are much larger than that of bare SS electrode, which indicates that the His derivatives have an effective protection on the SS surface. From Table 1, it can be found that the longer the assembling time, the larger the R_{ct} value, and the higher inhibition efficiency. The inhibition efficiency of the three kinds of SA films decreases as follows: Cbz-His > Ace-His > His. The maximal η values of His, Ace-His and Cbz-His self-assembled films are 90.32%, 91.87% and 94.24%, respectively. Due to the His and its derivatives molecules assembled on the SS surface to form a film which shields the SS surface from corrosion and makes the transition of SS/solution interface from a state of active dissolution to the passive state [50-56].

Compared with the Q_{dl} of each bare SS electrode and the SS electrode modified with His and its derivatives films, the Q_{dl} values almost decrease with the immersion time increasing. The double layer capacitance and the surface changes are in the relationship of inversely proportion. On the basis of Helmholtz model, the result is rational [57, 58]:

$$C_{dl} = \frac{\varepsilon_0 \varepsilon}{d} S \qquad (5)$$

where ε_0 and ε are both the dielectric constant but the difference is that ε_0 is the permittivity of air, ε is the permittivity of local, *d* is the thickness of the film and *S* is the electrode surface. Due to the inhibitor molecules which permittivity is lower replacement for water molecules assembled on the metal surface lead the C_{dl} value decreasing [59]. The decreasing of dielectric constant or an increasing of double-layer thickness can lead to the C_{dl} values. Because of the changing active sites there is a decrease in the surface area, so another reason that can cause C_{dl} decreasing is the changing active sites. These results show that His can inhibit the process and the adsorption at the metal-solution interface can precede the assembly molecules, all of which can prevent the metal from corrosion. The adsorption of the assembly molecules on the SS surface can be facilitated by the presence of hetero atoms (such as N, O) as well as aromatic ring [60-64]. His and its derivatives contain the N and O atoms which have some lone pair of electrons and the π-electron clouds in the aromatic rings. All of these can provide electrons to the unoccupied orbital of iron surface to form a stable coordination bonds. the His derivatives assembled on the SS surface decrease the part of SS surface exposed to shield the SS surface from the corrosion solution of NaCl. The n values in Table 1 are in the range of 0.775 to 0.881 with no rule. There is non-homogeneous surface for the working electrodes and there is no thick enough SA films to increase the heterogeneity, which can be the reason.

3.2. Polarization curves

The polarization curves of SS in 3.5% NaCl solution in the presence and absence of SA films with different assembly time ranged from 0 h to 12 h are shown in Fig. 3. With the immersion time increasing the corrosion rates become lower and the inhibition efficiencies become upper to the 3.5% NaCl solution without inhibitor. The immersion time, corrosion potential (E_{corr}), Tafel slopes and corrosion current density (I_{corr}) of electrochemical corrosion kinetics parameters are shown in Table 2. In this case, the inhibition efficiency is defined as follows:

$$\eta_{\mathrm{I}}(\%) = (1 - \frac{I^0_{\mathrm{corr}}}{I_{\mathrm{corr}}}) \times 100\% \qquad (6)$$

where I_{corr} is the corrosion current density in the uninhibited case and I^0_{corr} is the one in the inhibited case [65].

Table 2. Polarization parameters of different SA films modified SS electrodes in 3.5% NaCl solution.

Assembled molecules	Immersion time (h)	E_{corr} (V)	$-\beta_c$ (V dec^{-1})	B_a (V dec^{-1})	I_{corr} (10^{-8}A/cm^2)	η_{I} (%)
bare	0	-0.276	0.187	0.163	30.02	-
His	2	-0.316	0.160	0.156	11.49	61.73
	4	-0.344	0.159	0.145	6.976	76.76
	6	-0.350	0.146	0.124	5.942	80.21
	8	-0.338	0.135	0.107	4.459	85.15
	10	-0.329	0.125	0.099	3.590	88.04
	12	-0.324	0.117	0.095	2.928	90.25
Ace-His	2	-0.318	0.162	0.160	8.169	72.79
	4	-0.320	0.155	0.145	6.910	76.98
	6	-0.327	0.147	0.139	4.920	83.61
	8	-0.330	0.135	0.110	3.280	89.07

	10	-0.310	0.125	0.090	2.730	90.91
	12	-0.325	0.116	0.092	2.549	91.15
Cbz-His	2	-0.303	0.165	0.159	8.490	71.72
	4	-0.315	0.147	0.137	4.387	85.39
	6	-0.296	0.139	0.116	2.336	92.22
	8	-0.305	0.131	0.102	2.049	93.17
	10	-0.310	0.125	0.089	1.828	93.91
	12	-0.315	0.113	0.082	1.767	94.11

It is observed in Fig. 3 that the E_{corr} shifts to more negative values with the immersion time, which indicates that the His and its derivatives act as cathode inhibitors. In all conditions, the curves of the electrodes with the assembly inhibitor molecules become lower and the current density values decreases, which indicates that the SA films of three kinds of His and its derivatives reduce the dissolution rate of SS in 3.5% NaCl solution remarkably. The η values in Table 2 follow the order of Cbz-His > Ace-His > His which is inconsistent with the electrochemical impedance spectra.

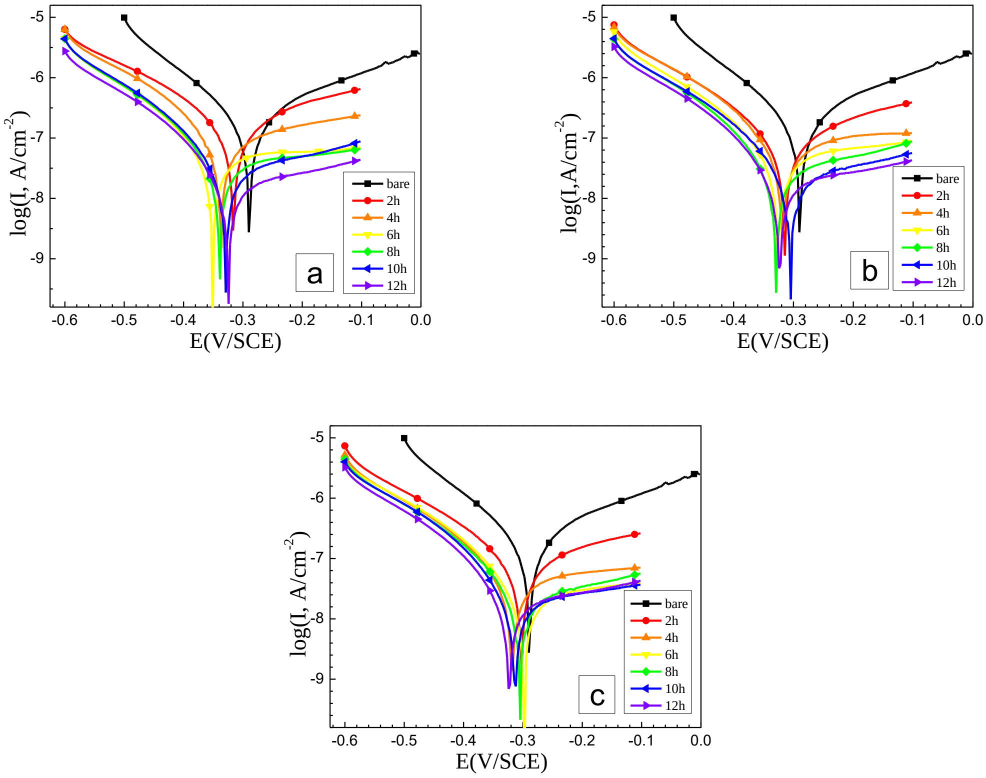

Figure 3. Polarization curves of His SA films covered SS electrodes formed in 0.01 His (a), 0.01 M Ace-His (b) and 0.01 M Cbz-His (c) solutions with different immersion time.

3.3 X-ray photoelectron spectroscopy (XPS)

The formation of surface coating is detected by X-ray photoelectron spectroscopy, exactly [66,67]. XPS is used to measure the Cbz-His SA film modified SS surface for further clarify the constituent. The XPS spectra were obtained from the SS surface treated by 0.01 M Cbz-His solution after 12 h of immersion. XPS spectra are shown in Fig. 4 and Fig. 5. The wide-scan XPS survey spectrum shows that the SA films contain the elements of being desired (Fig. 4). High-resolution XPS spectra of C 1s (Fig. 5a), N 1s (Fig. 5b), O 1s (Fig. 5c) and Fe 2p3/2 (Fig. 5d) regions of the Cbz-His SA films on SS surface are recorded to reveal the chemical states of C, N and O atoms in the SA films.

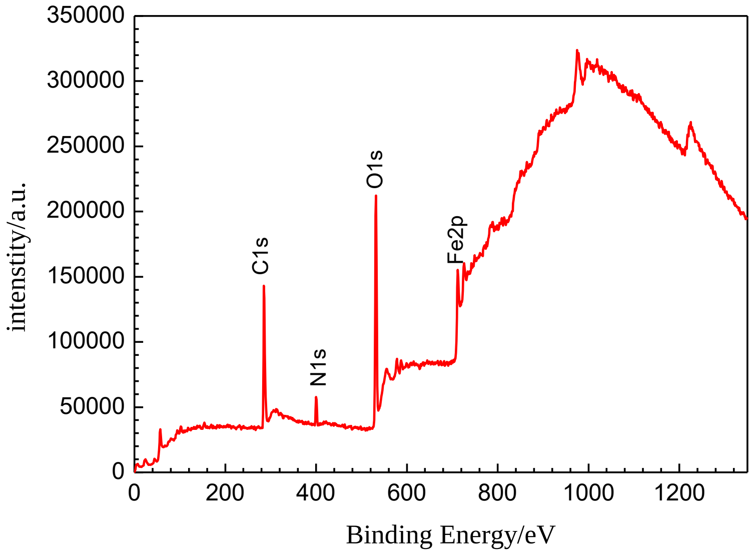

Figure 4. Wide-scan XPS spectrum of an Cbz-His modified SS surface.

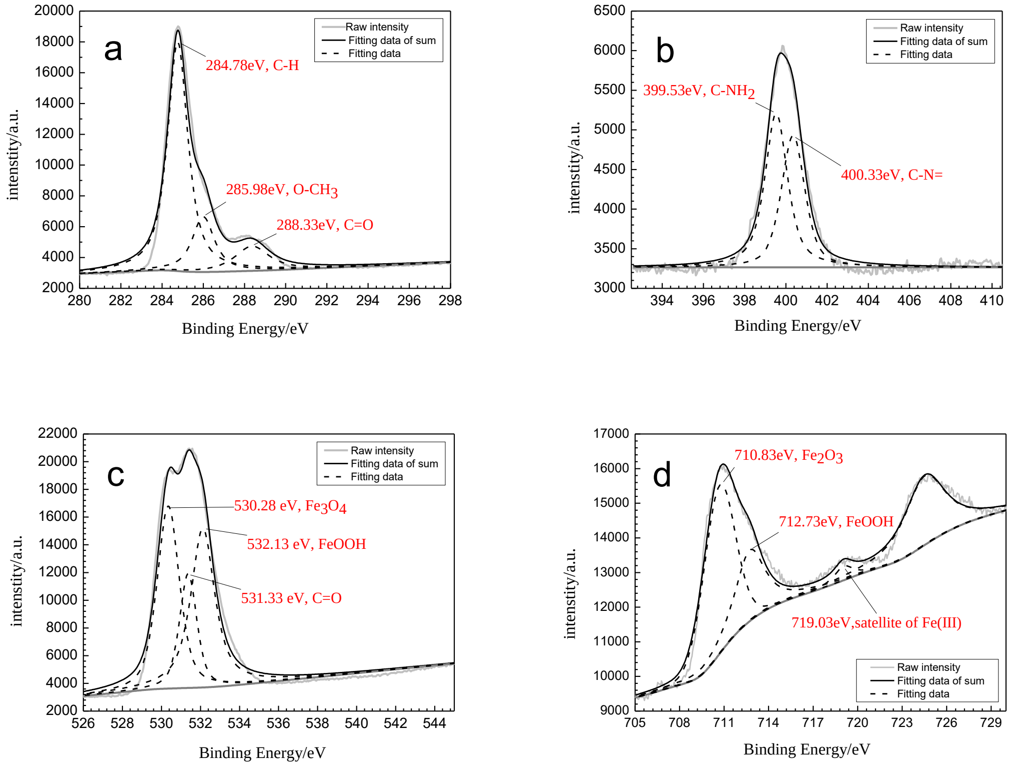

Figure 5. High-resolution XPS spectra for C1s (a), N1s (b), O1s (c) and Fe 2p3/2 (d).

The Fig. 5a of Wide-scan XPS spectrum shows the C 1s spectrum. The one peak is fitted into three peaks. The first fitted peak located about 284.78 eV belongs to the C-H and C-C [68]. The second fitted peak located at 285.98 eV belongs to the C-O or C-NH_2 [69]. The last fitted peak located about 288.33eV is high binding energy and it may belong to C=O [70]. The peak of N 1s for Cb-His assembled SS surface is shown in Fig. 5b. The one peak is fitted into two peaks. The one located at 399.53 eV is attributed to the bond of C-NH_2 and may be ascribed to the unprotonated N atom (=N-C structure) in the imidazole ring [71]. The other one located at 400.33 eV is ascribed to the coordinate nitrogen atoms in imidazole ring with steel surface (N-Fe) [72,73] and make the binding energy higher. The peak of O 1s spectrum with Cbz-His assembled on the SS surface is fitted into three peaks, too. The three fitted peaks are located at 530.23 eV, 532.13 eV and 531.33 eV, respectively. The first fitted peak is attributed to O^{2-}, and theoretically it is connected with the bond of Fe^{3+} in the Fe_2O_3 [74]. The second fitted peak belongs to the metal hydroxides or H_2O species (denoted Me-OH/H_2O) [75]. The third fitted peak may correspond to contain the C=O groups [76]. The peaks at 710.83 eV and 710.23 eV (Fig. 5d) are assigned to ferric compounds such as Fe_2O_3 and FeOOH, respectively [77, 78]. The peak at 710.23 eV may belong to the presence of FeOOH on the metal surface [79, 80]. The peak at 719.03 eV is attributed to the satellite of Fe (III) [78]. Obviously, from these results above, the Cbz-His molecules have been assembled on the SS surface.

3.4. Theoretical study

3.4.1 Quantum chemical calculations

The results of experiment confirm that the His and its derivatives can protect SS against corrosion in 3.5% NaCl solution via assembling on the SS surface. Quantum chemical calculations as an important research method are used to further investigate the interactions between the inhibitors and the SS surface. The frontier molecular orbital surfaces of the optimized molecules are shown in Fig. 6. The results of calculated quantum chemical contain the energy of the lowest unoccupied molecular orbital (E_{LOMO}), the energy of the highest occupied molecular orbital (E_{HOMO}) and the value of the energy gap ($\triangle E=E_{\mathrm{LOMO}}-E_{\mathrm{HOMO}}$) are shown in Table 3.

With low energy, higher E_{HOMO} Molecules can give electrons to the unfilled molecular orbital which is more suitable to accept it. On the contrary, a lower value shows that the negative charge can be suited by negative charge in the surface of the metal. Therefore, the decreasing of the energy gap ($\triangle E=E_{\mathrm{LOMO}}-E_{\mathrm{HOMO}}$) will cause the adsorption energy belong to inhibitors and iron surface to increase. Fig. 6 exhibits imidazole groups can cover the highest occupied molecular orbital (HOMO) in the surface, which shows that the coordination bond can give way to the absorption of iron surface. Moreover, the surface level on the benzyl (-Cbz) groups and the acetyl groups show that the back-donating bonds can adsorb the inhibitors on the surface of the iron. And the surface belongs to the lowest unoccupied molecular orbital (LUMO). The ΔE values in Table 3 follow the order of His > Ace-His > Cbz-, so that the η% of His and its derivatives follows the order of Cbz-His > Ace-His > His. However, E_{HOMO} values follow the order His > Ace-His > Cbz-His and E_{LUMO} follow the order of Cbz-His < Ace-His < His, which indicates that the aromatic rings (-Cbz groups) and the acetyl groups can not only improve the E_{HOMO} of the assembled molecules but also decrease the E_{LOMO} to improve the inhibition efficiency. The aromatic rings groups are better than the acetyl groups in improving the metal coordination of assembled molecules.

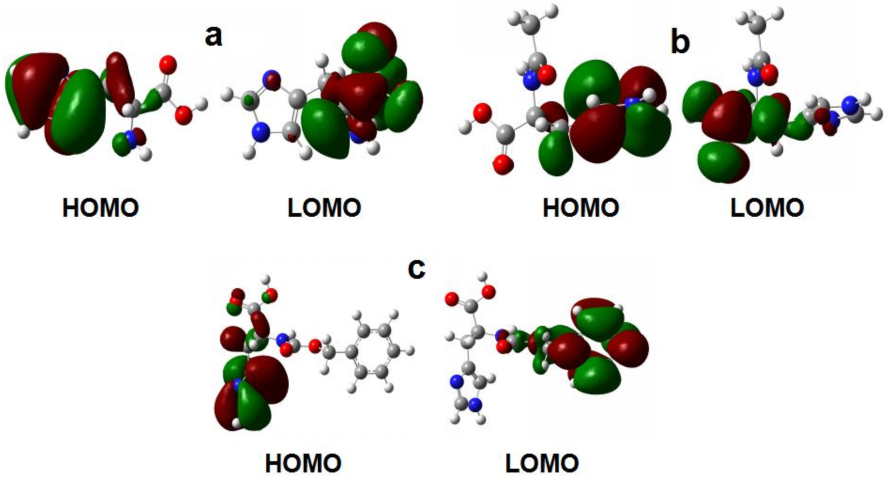

Figure 6. The frontier molecular orbital (EHOMO, ELOMO) surface of the Met (a), Ace-His (b) and Cbz-His (c) molecules.

Table 3. The calculating of quantum chemical parameters by using the B3LYP method and the 6-311G (d, p) basis, which is installed for His and its derivatives molecules.

Assembled molecules	E_{HOMO} (eV)	E_{LUMO} (eV)	$\triangle E$ (eV)	μ (Debye)
His	-6.027	-0.121	5.907	4.2207
Ace-His	-6.156	-0.342	5.813	3.4231
Cbz-His	-6.352	-0.583	5.769	5.8863

The different substituent functional groups lead to different chemical behavior. The Fukui function can prove the active sites of the His and its derivatives molecules. The active sites represent the reactive regions of a molecule so that it can show the mechanism of charge transfer [81-83, 84]. Show as in Table 4, the values f^{+} is maximum in absolute represent the locus in a molecule is liable to nucleophilic attack. Oppositely, where the values f^{-} is maximum in absolute is liable to electrophilic attack [84, 85]. The maximum absolute values of the f^{+} and f^{-} is shown in Table 4. The values are calculated via the Eq. (7) and Eq. (8):

$$f^{+} = q_{(\mathrm{N+1})} - q_{(\mathrm{N})} \qquad (7)$$

$$f^{-} = q_{(\mathrm{N})} - q_{(\mathrm{N-1})} \qquad (8)$$

where $q_{(\mathrm{N})}$ is the charges of the atoms with N electrons and $q_{(\mathrm{N+1})}$ is the atoms with one more electron (N+1) and $q_{(\mathrm{N-1})}$) is the atoms with one less electron (N-1).

Table 4. Setting the higher absolute values in the thery at the level of B3LYP/6-311G (d, p), Fukui functions of histidine and its derivatives can be selected.

	His			Ace-His			Cbz-His	
Atom	f^+	f^-	Atom	f^+	f^-	Atom	f^+	f^-
2C	-0.001	-0.234	1C	0.150	-0.241	1C	0.112	-0.203
3C	-0.160	-0.045	2C	0.023	-0.116	3C	-0.184	0.001
11C	0.073	-0.028	11C	0.103	-0.037	14N	0.068	-0.049
13C	-0.197	0.002	13C	-0.151	-0.002	20C	-0.176	0.084
17O	-0.243	-0.018	20C	-0.152	0.094	30C	-0.077	0.050

Seen from Fig. 1 and Table 4, the primary reactive sites about His and its derivatives for a nucleophilic attack are the carbon atoms, oxygen atoms of –C=O groups and 3C carbon atom of imidazole groups. The primary reactive sites for His and its derivatives for an electrophilic attack in most molecules are 1C and 2C carbon atoms of imidazole groups and some nitrogen atoms. The getting of *d*-orbitals of the metal can finish by the way of accepting and donating lone pair electrons. In all, the *d*-orbitals and these groups are the pivotal sites forming the coordinate bonds. The contrasting of the values belong to His and its derivatives and the Fukui function of different atoms , the result is that introducing acetyl groups and aromatic rings groups can improve the reactivity sites of assembly molecules, such as the 20C carbon atoms of Ace-His molecule and the 30C carbon atom of Cbz-His molecule.

3.4.2. Dynamic simulation

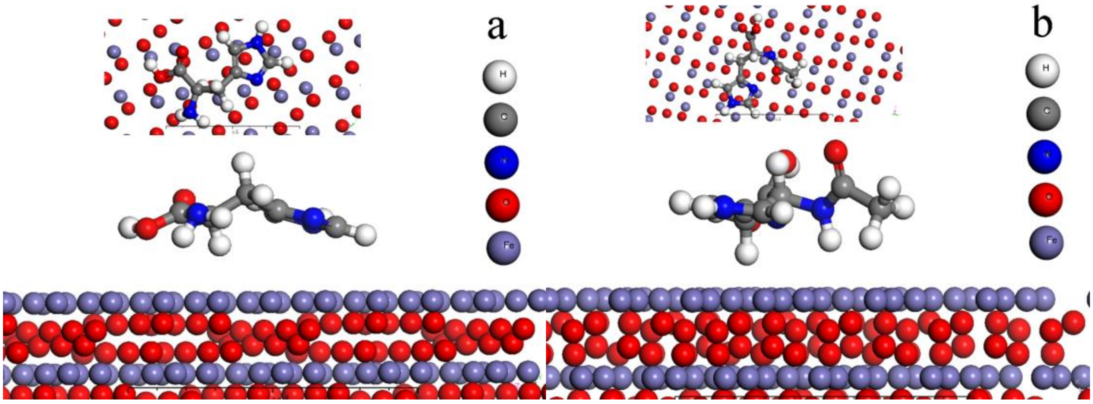

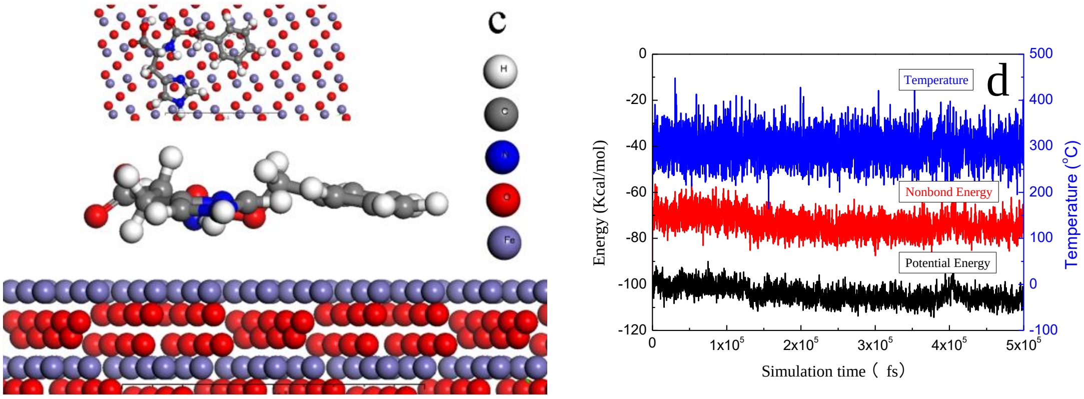

Figure 7. Equilibrium configuration of His and its derivatives molecules adsorbed on a Fe (1 1 0) surface, His (a), Ace-His (b) and Cbz-His (c), (d) is the temperature and energy fluctuation curves of the adsorption process of Cbz-His molecules on Fe_2O_3 (1 1 0) surface.

Molecular dynamics (MD) simulation was used to study the adsorption behavior of the His and its derivatives molecules on the SS surface. The equilibrium configuration of His and its derivatives molecules adsorbed on the Fe_2O_3 (1 1 0) surface are shown in Fig. 7. The energies of calculated binding and inhibition efficiencies of experimental are show in Table 5.

Table 5. Binding energies and inhibition efficiencies (η_{12h}) of His and its derivatives.

Assembled molecules	$E_{adsorption}$ eV	$E_{binding}$ eV	η_{12h} %
His	-1.193	1.193	90.32
Ace-His	-1.842	1.842	91.7
Cbz-His	-2.935	2.935	94.24

As can be seen from Fig. 7, the three kinds of His and its derivatives molecules are adsorbed on Fe_2O_3 (1 1 0) surface with a planar structure, these can be attributed to the relatively equal distribution of HOMO and LUMO densities on the whole molecule of His and its derivatives. Since the strength of physical interaction generally scales with the size of the molecule，this planar molecule surface attraction may enhance the physisorption by improving the van der Waals dispersion forces [24]. In addition, by the theoretical way, the binding energy and the stability of adsorptive system are in a close related relation. The effect of a stabler adsorption system and higher protection efficiency can get by the way of a higher binding energy. The $E_{binding}$ values in table 6 follows Cbz-His > Ace-His > His. The values of $E_{binding}$ in Table 6 follow the sequence of Cbz-His > Ace-His > His. It means that the Cbz-His molecule can easily absorb on Fe_2O_3 surface and protect it from corrosion. According to the quantum chemical calculations results, the His and its derivatives molecules may be adsorbed on the metal surface via the chemisorption mechanism by sharing the electrons between the reactive sites of assembled molecules and iron. The forming of coordinate bonds can be gotten by the way of the unoccupied *d*-orbital of iron to receive of the donated π-electrons and the forming of the anti-bonding orbital coordinate bonds by the electrons accepted from de-orbital of iron, all of which can cause the Aromatic rings groups (-Cbz group) and the acetyl groups to improve the adsorption capability of Cbz-His and Ace-His molecules on the Fe_2O_3 (1 1 0) skin layer. The aromatic rings groups is better than the acetyl groups in improving the metal coordination of assembled molecules due to the conjugation of aromatic ring and planar structure. The adsorptive stability of the derivatives as well as the inhibition efficiency increases with -Cbz group the in molecule structure. This is in good accordance with the experimental result where the inhibition efficiency follows the order of Cbz-His > Ace-His > His.

4. CONCLUSIONS

The corrosion inhibition investigation of His and its derivatives SA films on SS surfaces was carried out in 3.5% NaCl solutions. The primary results are as listed:

His and its derivatives could form SA films on SS surface and effectively inhibit it from corrosion in 3.5% NaCl solutions. The inhibition efficiency of all the SA films increased with the immersion time prolonged and the protection efficiency followed the order Cbz-His > Ace-His > His, the maximal protection efficiency was approximately 94.24%. XPS analyses indicated the Cbz-His molecules could adsorb on the SS surface and form SA films. The forming of coordinate bonds could be achieved by the way of accepting electrons from *d*-orbital of iron, and the forming of anti-bonding orbital coordinate bonds could be achieved by accepting electrons from *d*-orbital of iron. The absorption abilities of His molecule could be enhanced by introducing the aromatic rings groups (-Cbz group) and the acetyl groups which could be proved by quantum chemical calculations and dynamic simulations.

ACKNOWLEDGEMENTS
This work was funded by Guangxi Natural Science Foundation (2013GXNSFBA019212), the key project of science and technology research in universities of Guangxi (2013ZD029) and the Research Fund for the Guangxi Higher Education (2013YB114).

References

1. J. Zhang, G. Qiao, S. Hu, Y. Yan, Z. Ren, L. Yu, *Corros. Sci.*, 53 (2011) 147-152.
2. M. Mihit, S. El Issami, M. Bouklah, L. Bazzi, B. Hammouti, E. Ait Addi, R. Salghi, S. Kertit,*Appl. Surf. Sci.*, 252 (2006) 2389-2395.
3. J.M.T. M. S. Doescher, A. M. Rawlett, and M. L. Myrick, *J. Phys. Chem. B*, 105 (2001) 6.
4. H. Ge, H. Li, S. Mei, J. Liu, *Renew. Sust. Energ. Rev.*, 21 (2013) 331-346.
5. P.E.L. G. Kane Jennings, *Colloids Surf.*, 116 (1996) 10.
6. D.-q. Zhang, L.-x. Gao, G.-d. Zhou, *J. Appl. Electrochem.*, 35 (2005) 1081-1085.
7. I. Felhősi, E. Kálmán, *Corros. Sci.*, 47 (2005) 695-708.
8. H. Yang, J. Feng, Y. Liu, Y. Yang, J. Wu, Z. Zhang, G. Shen, R. Yu, *J. Raman Spectrosc.*, 36 (2005) 824-828.
9. K.A. Katsuhisa Nozawa, *Corros. Sci.*, 41 (1999) 17.
10. K. Aramaki, *Corros. Sci.*, 41 (1999) 16.
11. M. Foss, S. Diplas, E. Gulbrandsen, *Electrochim. Acta*, 55 (2010) 4851-4857.

12. A.-R. El-Sayed, U. Harm, K.-M. Mangold, W. Fürbeth, *Corros. Sci.*, 55 (2012) 339-350.
13. R.K. Shervedani, A. Hatefi-Mehrjardi, M.K. Babadi, *Electrochim. Acta*, 52 (2007) 7051-7060.
14. H. Ashassi-Sorkhabi, M.R. Majidi, K. Seyyedi, *Appl. Surf. Sci.*, 225 (2004) 176-185.
15. N.H. K.F. Khaled, *Electrochim. Acta*, 48 (2003) 9.
16. S.A.M. Refaey, F. Taha, A.M. Abd El-Malak, *Appl. Surf. Sci.*, 236 (2004) 175-185.
17. T. Shimura, K. Aramaki, *Corros. Sci.*, 50 (2008) 596-604.
18. T. Shimura, K. Aramaki, *Corros. Sci.*, 50 (2008) 1397-1405.
19. T. Shimura, K. Aramaki, *Corros. Sci.*, 50 (2008) 2407-2414.
20. M. Ehteshamzade, T. Shahrabi, M.G. Hosseini, *Appl. Surf. Sci.*, 252 (2006) 2949-2959.
21. D.-Q. Zhang, Q.-R. Cai, X.-M. He, L.-X. Gao, G.S. Kim, *Mater. Chem. Phys.*, 114 (2009) 612-617.
22. E.E. Oguzie, Y. Li, F.H. Wang, *J. Colloid Interface Sci.*, 310 (2007) 90-98.
23. E.E. Oguzie, Y. Li, F.H. Wang, *Electrochim. Acta*, 52 (2007) 6988-6996.
24. Z. Zhang, N. Tian, L. Zhang, L. Wu, *Corros. Sci.*, 98 (2015) 438-449.
25. K.Y. El-Baradie, N.A. El-Wakiel, H.A. El-Ghamry, *Appl. Organomet. Chem.*, 29 (2015) 117-125.
26. J.-j. Fu, S.-n. Li, Y. Wang, L.-h. Cao, L.-d. Lu, *J. Mater. Sci.*, 45 (2010) 6255-6265.
27. M. Bobina, A. Kellenberger, J.-P. Millet, C. Muntean, N. Vaszilcsin, *Corros. Sci.*, 69 (2013) 389-395.
28. D.-Q. Zhang, X.-M. He, Q.-R. Cai, L.-X. Gao, G.S. Kim, *Thin Solid Films*, 518 (2010) 2745-2749.
29. M. Mobin, M. Parveen, M.Z.A. Rafiquee, *J. Mater. Eng. Perform.*, 22 (2012) 548-556.
30. M. J. Frisch, G. W. Trucks, H. B. Schlegel, G. E. Scuseria, M. A. Robb, J. R. Cheeseman, J. A. Montgomery, Jr., T. Vreven, K. N. Kudin, J. C. Burant, J. M. Millam, S. S. Iyengar, J. Tomasi, V. Barone, B. Mennucci, M. Cossi, G. Scalmani, N. Rega, G. A. Petersson, H. Nakatsuji, M. Hada, M. Ehara, K. Toyota, R. Fukuda, J. Hasegawa, M. Ishida, T. Nakajima, Y. Honda, O. Kitao, H. Nakai, M.Klene, X. Li, J. E. Knox, H. P. Hratchian, J. B. Cross, C. Adamo, J. Jaramillo, R. Gomperts, R.E. Stratmann, O. Yazyev, A. J. Austin, R. Cammi, C. Pomelli, J. W. Ochterski, P. Y. Ayala, K. Morokuma, G. A. Voth, P. Salvador, J. J. Dannenberg, V. G. Zakrzewski, S. Dapprich, A. D. Daniels, M. C. Strain, O. Farkas, D. K. Malick, A. D. Rabuck, K. Raghavachari, J. B. Foresman, J. V. Ortiz, Q. Cui, A. G. Baboul, S. Clifford, J. Cioslowski, B. B. Stefanov, G. Liu, A. Liashenko, P. Piskorz, I. Komaromi, R. L. Martin, D. J. Fox, T. Keith, M. A. Al-Laham, C. Y. Peng, A. Nanayakkara, M. Challacombe, P. M. W. Gill, B. Johnson, W. Chen, M. W. Wong, C. Gonzalez, and J. A. Pople, Gaussian, Inc., Wallingford CT, 2004.
31. A.D. Becke, *Phys. Rev. A*, 38 (1988): 3098-3100.
32. C. Lee, W. Yang, R.G. Parr, *Phys. Rev.*, 37 (1988):785–789.
33. A.D. Becke, *J. Chem. Phys.*, 98 (1993): 5648–5652.
34. J. Barriga, B. Coto, B. Fernandez, *Tribol. Int.*, 40 (2007) 960-966.
35. H. Hosokawa, M. Nagase, *J. Nucl. Sci. Technol.*, 41 (2004) 682-689.
36. M. Morales, J.M. Chimenos, F. Espiell, M. Segarra, *Surf. Coat. Technol.*, 238 (2014) 51-57.
37. S.U. Rahman, *Surf. Coat. Technol.*, 205 (2011) 3035-3042.
38. S.B. N.E. Hakiki, B. Rondot and M. Da Cunha Belo, *Corros. Sci.*, 37 (1995) 14.
39. W. Su, Y. Tian, S. Peng, *Appl. Surf. Sci.*, 315 (2014) 95-103.
40. S. Zhang, L. Jia, T. Yu, *Electrochim. Acta*, 89 (2013) 253-261.
41. G. Golestani, M. Shahidi, D. Ghazanfari, *Appl. Surf. Sci.*, 308 (2014) 347-362.
42. S.Maximovitch, *Electrochim. Acta*, 41 (1996) 11.
43. L. Jinlong, L. Hongyun, *Appl. Surf. Sci.*, 263 (2012) 29-37.
44. K.F. Khaled, *J. Solid. State. Electr.*, 13 (2009) 1743-1756.
45. S.C. H. Ma, L. Niu, S. Zhao, S. Li and D. Li, *J. Appl. Electrochem.*, 32 (2002) 8.
46. H. Ashassi-Sorkhabi, E. Asghari, *Electrochim. Acta*, 54 (2008) 162-167.
47. B. Hirschorn, M.E. Orazem, B. Tribollet, V. Vivier, I. Frateur, M. Musiani, *J. Electrochem. Soc.*, 157 (2010) C458.
48. B. Hirschorn, M.E. Orazem, B. Tribollet, V. Vivier, I. Frateur, M. Musiani, *Electrochim. Acta*, 5

(2010) 6218-6227.

49. C. H. Hsu and F. Mansfeld, *Corrosion*, 57(2001), 747-748.
50. E. Oró, A. de Gracia, A. Castell, M.M. Farid, L.F. Cabeza, *Appl. Energ.*, 99 (2012) 513-533.
51. S. Guillot, A. Faik, A. Rakhmatullin, J. Lambert, E. Veron, P. Echegut, C. Bessada, N. Calvet, X. Py, *Appl. Energ.*, 94 (2012) 174-181.
52. A.-S. Duwez, *J. Electron Spectrosc. Relat. Phenom.*, 134 (2004) 97-138.
53. G. Li, Y. Hwang, R. Radermacher, *Int. J. Refrig.*, 35 (2012) 2053-2077.
54. T.H. Degefa, P. Schön, D. Bongard, L. Walder, *J. Electroanal. Chem.*, 574 (2004) 49-62.
55. P. Ramírez, R. Andreu, J.J. Calvente, C.J. Calzado, G. López-Pérez, *J. Electroanal. Chem.*, 582 (2005) 179-190.
56. B.M. M. Lagrenee, M. Bouanis, M. Traisnel, F. Bentiss, *Corros. Sci.*, 44 (2002) 16.
57. B.M. M. Lagrenee, M. Bouanis, M. Traisnel, F. Bentiss, *Corros. Sci.*, 44 (2002) 16.
58. E. McCafferty. Introduction to Corrosion Science, Springer, New York, Dordrecht, Heidelberg, London, New York, 2010.
59. A. Kosari, M.H. Moayed, A. Davoodi, R. Parvizi, M. Momeni, H. Eshghi, H. Moradi, *Corros. Sci.*, 78 (2014) 138-150.
60. A. Yurt, G. Bereket, C. Ogretir, *J. Mol. Struct.*, 725 (2005) 215-221.
61. D.-Q. Zhang, B. Xie, L.-X. Gao, Q.-R. Cai, H.G. Joo, K.Y. Lee, *Thin Solid Films*, 520 (2011) 356-361.
62. N.O. Eddy, *J. Adv. Mater. Res.*, 2 (2011) 35-47.
63. A. Rochdi, R. Touir, M.E. Bakri, M. Ebn Touhami, S. Bakkali, B. Mernari, *J. Environ. Chem. Eng.*, 3 (2015) 233-242.
64. H. Bhandari, R. Srivastav, V. Choudhary, S.K. Dhawan, *Thin Solid Films*, 519 (2010) 1031-1039.
65. M.T.b. F. Bentiss a , M. Lagrenee, *Corros. Sci.*, 42 (2000) 20.
66. I.V. Sieber, H. Hildebrand, S. Virtanen, P. Schmuki, *Corros. Sci.*, 48 (2006) 3472-3488.
67. I. Díez-Pérez, C. Vericat, P. Gorostiza, F. Sanz, *Electrochem. Commun.*, 8 (2006) 627-632.
68. N.A. Odewunmi, S.A. Umoren, Z.M. Gasem, *J. Environ. Chem. Eng.*, 3 (2015) 286-296.
69. M. Outirite, M. Lagrenée, M. Lebrini, M. Traisnel, C. Jama, H. Vezin, F. Bentiss, *Electrochim. Acta*, 55 (2010) 1670-1681.
70. N.A. Odewunmi, S.A. Umoren, Z.M. Gasem, *J. Ind. Eng. Chem.*, 21 (2015) 239-247.
71. H. Nahali, L. Dhouibi, H. Idrissi, *Constr Buld Mater*, 78 (2015) 92-101.
72. L.T. Weng, C. Poleunis, P. Bertrand, V. Carlier, M. Sclavons, P. Franquinet, R. Legras, *J. Adhes. Sci.Technol.*, 9 (1995) 859-871.
73. O. Olivares, N.V. Likhanova, B. Gómez, J. Navarrete, M.E. Llanos-Serrano, E. Arce, J.M. Hallen,*Appl. Surf. Sci.*, 252 (2006) 2894-2909.
74. W. Temesghen, P.M. Sherwood, *Anal. Biochem.*, 373 (2002) 601-608.
75. C.M. Abreu, M.J. Cristóbal, R. Losada, X.R. Nóvoa, G. Pena, M.C. Pérez, *Electrochim. Acta*, 51 (2006) 2991-3000.
76. C.L. Ksenija Babic-Samardz ija, Norman Hackerman, Andrew R. Barron, and Andreas Luttge,*Langmuir*, 21 (2005) 10.
77. M.A. Pech-Canul, P. Bartolo-Pérez, *Surf. Coat. Technol.*, 184 (2004) 133-140.
78. B. Zeybek, E. Aksun, *Prog. Org. Coat.*, 81 (2015) 1-10.
79. N. Narimani, B. Zarei, H. Pouraliakbar, G. Khalaj, *Meas. Sci. Technol.*, 62 (2015) 97-107.
80. S.A. Kusmanov, A.A. Smirnov, Y.V. Kusmanova, P.N. Belkin, *Surf. Coat. Technol.*, (2014).
81. L. Herrag, B. Hammouti, S. Elkadiri, A. Aouniti, C. Jama, H. Vezin, F. Bentiss, *Corros. Sci.*, 52 (2010) 3042-3051.
82. I.B. Obot, N.O. Obi-Egbedi, *Corros. Sci.*, 52 (2010) 198-204.
83. M.K. Pavithra, T.V. Venkatesha, M.K. Punith Kumar, H.C. Tondan, *Corros. Sci.*, 60 (2012) 104-111.
84. X. Li, X. Xie, S. Deng, G. Du, *Corros. Sci.*, 87 (2014) 27-39.

85. H. Zhao, X. Zhang, L. Ji, H. Hu, Q. Li, *Corros. Sci.*, 83 (2014) 261-271.